NANO LETTERS

2008
Vol. 8, No. 4
1026-1032

# Experimental and Theoretical Studies Suggesting the Possibility of Metallic Boron Nitride Edges in Porous Nanourchins

**M. Terrones,[*,†,‡] J.-C. Charlier,[*,§] A. Gloter,[‡,||] E. Cruz-Silva,[†] E. Terrés,[†,⊥] Y. B. Li,[#] A. Vinu,[‡,▽] Z. Zanolli,[§] J. M. Dominguez,[||] H. Terrones,[†] Y. Bando,[‡,#,▽] and D. Golberg[*,#,▽]**

*Advanced Materials Department, IPICYT, Camino a la Presa San José 2055, Col. Lomas 4 sección, San Luis Potosí, 78216, México, International Center for Young Scientists (ICYS), National Institute for Materials Science, Namiki 1-1, Tsukuba, Ibaraki 305-0044, Japan, Université Catholique de Louvain, Unité de Physico-Chimie et Physique des Matériaux (PCPM), European Theoretical Spectroscopy Facility (ETSF), B-1348 Louvain-la-Neuve, Belgium, Laboratoire de Physique des Solides, CNRS UMR 8502, Université Paris-Sud, Orsay, 91405, France, Programa de Ingeniería Molecular, Instituto Mexicano del Petróleo, Eje Central Lázaro Cárdenas 152, México, D.F., C.P. 07730, México, Nanoscale Materials Center, National Institute for Materials Science, Namiki 1-1, Tsukuba, Ibaraki 305-0044, Japan, and International Center for Materials Nanoarchitectonics, World Premier International Research Center, National Institute for Materials Science, Namiki 1-1, Tsukuba, Ibaraki 305-0044, Japan*

*Received October 20, 2007; Revised Manuscript Received January 23, 2008*

## ABSTRACT

**We first describe the synthesis of novel and highly porous boron nitride (BN) nanospheres (100–400 nm o.d.) that exhibit a rough surface consisting of open BN nanocones and corrugated BN ribbons. The material was produced by reacting $B_2O_3$ with nanoporous carbon spheres under nitrogen at ca. 1750 °C. The BN nanospheres were characterized using scanning electron microscopy, high-resolution electron microscopy, and electron energy loss spectroscopy. The porous BN spheres show relatively large surface areas of ca. 290 $m^2/g$ and exhibit surprisingly stable field emission properties at low turn-on voltages (e.g., 1–1.3 V/$\mu$m). We attribute these outstanding electron emission properties to the presence of finite BN ribbons located at the surface of the nanospheres (exhibiting zigzag edges), which behave like metals as confirmed by first-principles calculations. In addition, our ab initio theoretical results indicate that the work function associated to these zigzag BN ribbons is 1.3 eV lower when compared with BN-bulk material.**

Hexagonal boron nitride (BN) is an insulating layered material with a structure analogous to graphite that exhibits a large band gap of ca. 5.5. eV. Similar to graphite, BN is able to bend and curl so as to form fullerene-like structures[1] and nanotubes.[2] Numerous advances in the synthesis of BN nanotubes have been achieved over the last 10 years.[3] For example, BN nanotubes are now produced using arc-discharge techniques,[4–6] chemical vapor deposition (CVD) methods,[2] substitution reactions,[7] ball milling,[8,9] laser ablation,[10] etc.

It has been demonstrated experimentally that BN nanotubes are able to emit electrons from their tips under extremely large electric fields.[11] However, layered BN could adopt novel morphologies and could exhibit different properties when compared to bulk BN or BN nanotubes. In this Letter we describe the synthesis of a novel form of porous

* To whom correspondence should be addressed: mterrones@ipicyt.edu.mx, Jean-Christophe.Charlier@uclouvain.be, GOLBERG.Dmitri@nims.go.jp.
† Advanced Materials Department, IPICYT.
‡ International Center for Young Scientists (ICYS), National Institute for Materials Science.
§ Université Catholique de Louvain, Unité de Physico-Chimie et Physique des Matériaux (PCPM).
|| Laboratoire de Physique des Solides, CNRS UMR 8502, Université Paris-Sud.
⊥ Programa de Ingeniería Molecular, Instituto Mexicano del Petróleo.
# Nanoscale Materials Center, National Institute for Materials Science.
▽ International Center for Materials Nanoarchitectonics, World Premier International Research Center, National Institute for Materials Science.

10.1021/nl072713m CCC: $40.75 
**Published on Web 03/12/2008**

BN nanospheres that consist of interconnected BN channels in the core, in addition to open BN nanocones and protruding BN ribbons on their surface. By studying their field emission properties, we noted surprising emission currents occurring at low-turn-on voltages (1–1.3 V/$\mu$m). We attribute these results to the presence of open BN edges located on the nanoball surface. We further performed ab initio calculations and confirmed that BN ribbons (exhibiting zigzag edges) could behave as metals. The corresponding work function is predicted to be 1.3 eV lower compared to BN bulk material, confirming the enhancement of the field emission properties in these BN ribbons. Therefore, and to the best of our knowledge, this constitutes the first report on the possibility of finding a form of metallic BN. We envisage that individual BN nanoribbons could now be used in the fabrication of nanoelectronic devices operating at high temperatures under oxidating conditions. In addition, these novel porous BN architectures could lead to other fascinating materials such as catalysts and high surface area gas storage components that could substitute activated carbons.

Our nanoporous carbon structures were prepared using mesoporous spherical silica (MCM 48) as a template.[12] One gram of spherical MCM-48 was added to a solution consisting of 1.25 g of sucrose ($C_{12}H_{22}O_{11}$ Aldrich, 99%), 0.07 mL of $H_2SO_4$ (Merck, 98%), and 6 mL of $H_2O$. The mixture was then dried for 6 h at 100 °C in $N_2$ and at 160 °C for additional 6 h. A second impregnation process was repeated, and the silicate was then dried and pyrolyzed at 1000 °C in Ar for 1 h. The products were then stirred in 48 wt % aqueous HF for 30 min in order to remove silicate template and filtered under vacuum.

Subsequently, 20 mg of spherical nanoporous carbon particles was placed in the center of a graphite disk (15 mm diameter) containing a little dip in the middle, and numerous perforations of 1.5 mm diameter around. The disk was fitted into a cylindrical graphite crucible, which contained 400 mg of $B_2O_3$ powder (Aldrich Co.) at the bottom. The crucible was then slowly heated to ca. 1700 °C under a $N_2$ flow (ca. 2–3 L/min) inside a high-frequency induction furnace.[13] The resulting material was subsequently annealed for 30 min in a $N_2$ flow, and the samples were allowed to cool to room temperature.

The products were characterized using a powder X-ray diffractometer at low angles ($2\theta = 1$–$10°$; Siemens D-500 using Cu K$\alpha$ radiation, $\lambda = 0.1548$ nm). High-resolution transmission electron microscopy (HRTEM) studies were performed with a JEOL field-emission microscope, JEOL-3000F, operated at 300 kV, equipped with a Gatan 766 electron energy loss spectrometer, 2D-DigiPEELS, and a high-resolution energy-filtered field-emission transmission electron microscope (HRTEM, JEOL-3100F; Omega filter) with an estimated spatial resolution on the energy-filtered images of ca.1.0 nm. The pore structure of the samples was determined at 77 K with an automatic volumetric sorption analyzer Autosorb-1C using $N_2$ as the adsorbent. The specific surface area and the total pore volume were determined from the BET equation and the volume of $N_2$ adsorbed at a relative pressure of 0.99. The pore size distribution was obtained from the adsorption branch of the isotherm using the Barret–Joyner–Halenda (BJH) method.

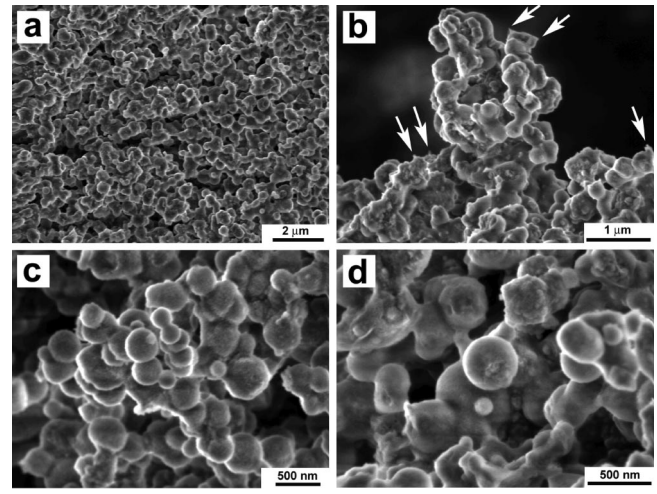


**Figure 1.** SEM images of BN nanospheres produced in this study under different magnifications. It is noteworthy to mention that the surfaces of these nanoballs exhibit protuberances (b).

Field-emission measurements on the BN nanosphere material were carried out in a standard microfilm emission device. Approximately 10 mm × 10 mm surface area of a BN nanosphere powder was attached to conductive sticky tape and tightly pressed with a glass slider. No attempt was made to align the structures. A small fraction of the spheres protrudes from the film and extend their tips outwardly, up to several micrometers above the surface. The macrofilm field-emission characteristics were measured in a chamber evacuated to ca. $10^{-8}$ Torr. A local zero spacing between the sample surface and the anode electrode (Al rod; 1.2 mm in diameter) was precisely determined via biasing the Al anode to ca. 0.5 V and moving it toward the film surface until a marginal contact current was recorded with a Keithley-237 device; then the film–anode spacing was accurately adjusted with the aid of a goniometer stage having a 5 $\mu$m step. During the experiments, the nanosphere film–anode spacing ranged between 220 and 270 $\mu$m, and the anode was gradually biased up to 1100 V during the continuous recording of $I-V$ curves.

Scanning electron microscopy (SEM) images of the BN material shows the presence of uniform spherical balls ranging from 100 to 400 nm in diameter (Figure 1). The spheres usually agglomerate and stick to one another. In some cases one could observe coalesced balls. It is interesting to note that the surface of spheres exhibits various protuberances (see arrows in Figure 1b). TEM observations of the BN powder revealed the presence of porous, spiky, and corrugated spheres exhibiting protruding ribbons and edges (Figure 2a). The surface shown in Figure 2a is very similar to the surface observed by SEM (Figure 1b). A closer inspection of the center of the sphere reveals interlinked BN layers that form cavities (pores). These cavities are attributed to the porous nature of the spheres (Figure 2b). Figure 2c depicts a TEM image of the edge of one of the spheres showing ribbon-like material protruding from the surface of the sphere. These ribbons were always observed and appear

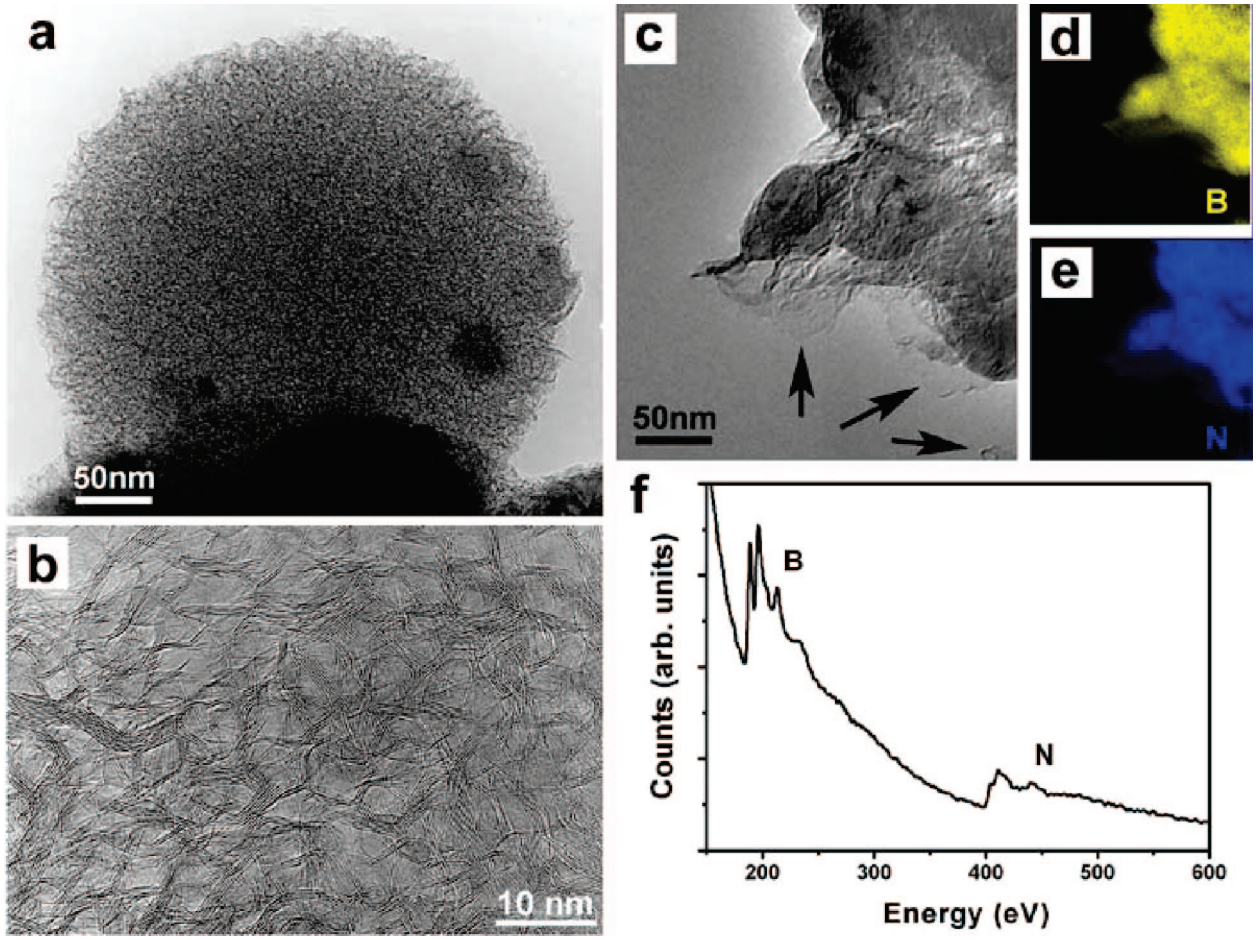


**Figure 2.** (a) TEM image of a typical BN nanoball showing a "spiky" and a porous-like morphology. (b) HRTEM image of the inner core of (A) revealing the presence of interlinked BN layers that form cavities (pores). The layers usually consist of two to six BN stacked sheets. (c) TEM image of the surface of one BN nanoball exhibiting exposed layers of BN material. (d, e) Elemental mapping for B and N, respectively, demonstrating that the material consists of B and N only (Supporting Information shows that C or O are absent in these samples). (f) EEL spectrum of a typical BN nanosphere showing the presence of B and N sharp edges located at ca. 188 and 401 eV, respectively.

to have some open edges that are clearly exposed (Figure 2c and Supporting Information). It is possible that the BN ribbon edges are hydrogen terminated; note that the samples were exposed to air and that H atoms cannot be detected by electron energy loss spectroscopy (EELS) or energy dispersive X-ray spectroscopy.

An elemental mapping of a typical nanosphere, using EELS, is depicted in panels d and e of Figure 2. Here we could clearly observe that the nanoballs are made of B and N only (see Figures S1−S3 in Supporting Information). We should note that when observation times are long under the TEM, elemental C could be found due to beam contamination effects, a phenomenon that is commonly observed during TEM observations. The growth of these BN nanourchin materials is attributed to the reaction of $B_2O_3$ with nitrogen and the pure carbon balls. It has been previously demonstrated by Golberg et al.[14] that the complete substitution of C by B and N could be achieved if the reaction temperature is high enough (as in our case). We also observed an incomplete substitution of the C atoms in the porous spheres when lower temperatures (e.g., <1600 °C) were used (results not shown here). Interestingly, we never managed to witness any electron emission from the material (possibly because the BCN behaves as a semiconductor and is not a good field emitter). The detailed growth and the formation mechanism of these BN and BCN structures will be reported elsewhere. Various EEL spectra on the BN porous nanostructures revealed the presence of only B and N. The spectra showed energy loss edges located at ca. 188 and 401 eV. These correspond to excitations of the K-shell electrons of B and N, respectively (Figure 2f).

HRTEM studies of the surfaces of the spheres revealed the presence of stacked and open ribbons consisting of interlinked layered material identified as pure BN layers from EELS measurements (Figure 3). HRTEM images of the inner core of the BN spheres exhibited notorious interlinking of curved BN layers (porous-like, typically between 2 and 4 BN layers; Figure 2b and Figures S4−S6, S9, and S10). A closer inspection of the outer surface of the spheres indicates the presence of exposed BN edges arising from unfolded ribbons (Figure 3 and Figures S5, S7, and S8). These unfolded edges provide the spiky morphology of the spheres, and it is believed that the bare BN edges will provide a high reactivity of the BN spheres which could be useful in the development of sensors, catalysts, field emission devices, and ceramic composites (Figures S7 and S8).

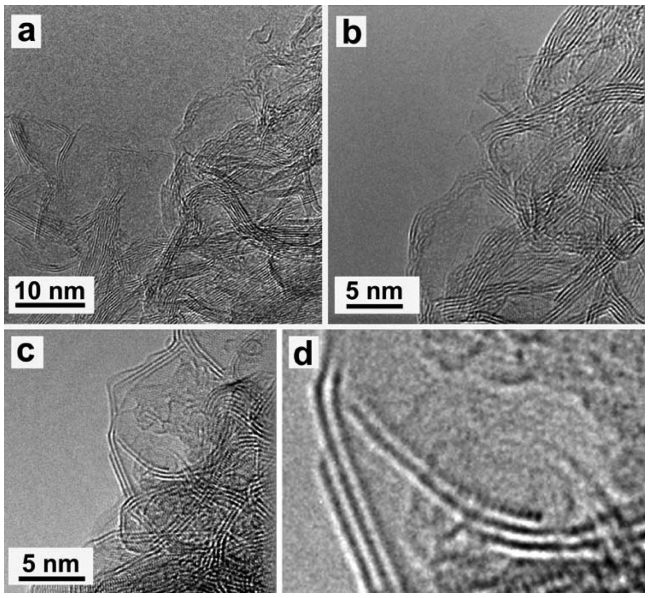


**Figure 3.** HRTEM images of the outer surfaces of the BN nanospehers. One could easily observe that BN layers protrude from their surfaces. These layers consist of BN and have clear exposing edges. The image depicted in panel d shows a higher magnification of panel c, which clearly reveals the hexagonal pattern of BN. In addition, one could clearly see the presence of exposed layers.

It is noteworthy that these ribbons consist of at least two stacked BN layers. In some occasions, we could observe the hexagonal lattice of the ribbons using HRTEM (see right-hand side in Figure 3d). In addition to these edges, the presence of open and closed BN cones was also observed (not shown here). Similarly to the open edges, these conelike morphologies would be more reactive, thus making the material very attractive for nanotechnological applications.

In order to demonstrate the high surface area of these BN nanospheres, we carried out $N_2$ adsorption measurements and found a BET surface of ca. 290 $m^2/g$, a value which is extremely high for BN (at least twice as much as the numbers reported for activated BN). In particular, these activated BN have shown surface area values of 168 $m^2/g$.[15] The pore size distribution of our BN spheres, determined using the BJH method, indicated an average value of 3.3 nm (see Figure S11 in Supporting Information). However, pore sizes of between 2.0 and 2.5 nm were also present in the samples. It is important to note that the nanoporous carbon material, used as a template for producing these BN nanospheres, exhibited pore sizes of 2.1 nm and pore volumes between 2.5 and 4 $cm^3/g$.[16] Therefore, the BN material possesses different characteristics when compared to the pure carbon counterpart. Due to the high surface area and the relatively small pore size, observed for these BN nanospheres, it is possible that the material could be very attractive for making $H_2$ storage components. In addition, experimental and theoretical work have demonstrated efficient physical adsorption of $H_2$ on defective BN nanotubes; defective BN nanostructures and exposed BN sheets tend to adsorb more $H_2$ molecules.[17–20] For these reasons, we believe that our BN nanourchin structures, which exhibit high surface areas,

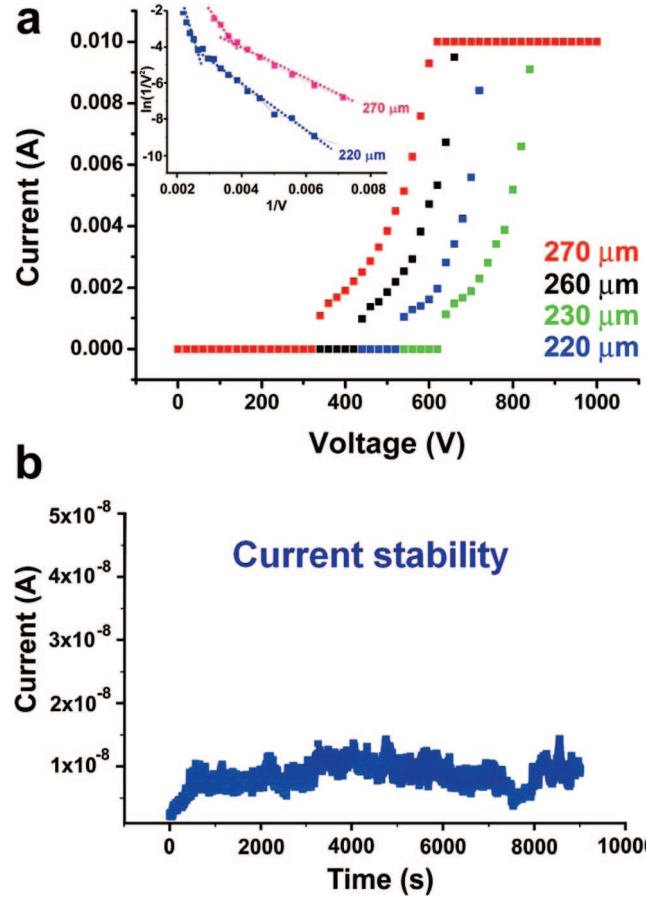


**Figure 4.** (a) Typical field-emission *I–V* curves obtained on the BN nanoball material. It is clear that the films consisting of BN nanoballs exhibit low turn-on voltages of 1.1−1.3 V/$\mu$A (i.e., those corresponding to 10 $\mu A/cm^2$); the F−N plots for the 220 and 270 $\mu$m film-anode spacings are shown in the inset; those display two various slopes for the low- and high-voltage regions. (b) Current stability of the BN nanosphere films showing relatively stable electron emission in time. It is noteworthy that the emission increased linearly in the first stage of the process, possibly due to the fact that some foreign species located on the exposed BN edges of the balls were removed by the presence of an electric field.

defects, and exposed edges, are likely to adsorb $H_2$ efficiently. Complementary $H_2$ storage measurements are currently underway.

The bulk field-emission characteristics from macrofilms consisting of these spiky BN nanoballs are depicted in Figure 4. The anode−film spacing was consecutively decreased from 270 to 220 $\mu$m, at steps of 10 $\mu$m for the BN nanoball material. We observed low-turn-on fields, defined here as those necessary to produce a current density of 10 $\mu A/cm^2$. In particular, we noted turn-on fields ranging from 1.1 to 1.3 V/$\mu$m (Figure 4). This result is quite unexpected, because bulk BN is an insulating material and emission could start only at high voltages. For example, polycrystalline BN films exhibit turn-on voltages in the range of 15.2−8.3 V/$\mu$m.[21] The values reported here approach the lowest ones obtained for conventional C nanotube field-emitting films (1–3 V/$\mu$m).[22,23] From these results, we could state that the electron emission could be occurring from the BN open edges and protuberances present on the surface of the nanospheres

which can be clearly observed in Figures 1b, 2c, and 3 (see also Figures S5, S7, and S8).

We should emphasize that the BN nanosphere film emissions became more stable a few seconds after applying the voltage. This effect could be due to the fact that the surface of the as-produced balls, consisting of BN ribbons, was saturated or passivated with foreign species (e.g., hydrogen, oxygen, etc.) that inhibited electron emission. Once the species located at the edges of the ribbons are removed by the electric field, it is natural to expect an enhanced and more constant emission current. In our BN spiky spheres, we observed reasonable current stability for 9000 s (Figure 4b; we stopped the emission at this point because we did not observe drastic changes in the current stability). Interestingly, we also distinctly observed two regions with various slopes on the Fowler−Nordheim (F−N) plots. The slopes drastically increased while the bias voltages reached ~300 V (Figure 4 inset; F−N plots for 220 and 270 $\mu$m).

We should also emphasize that for *carbon containing BN nanospheres* (produced at temperatures lower than 1700 °C and shorter reaction times), we never observed any stable emission due to fact that BCN materials tend segregate into BN and C domains and are much more unstable when compared to pure BN systems. We noted that the BCN material was only shorting during electron emission (results not shown here). Therefore, the presence of C atoms into BN does not favor stable field emission. This result suggests once more that our pure BN material (more stable than BCN or $BC_2N$) could indeed have metallic edges that efficiently emit electrons (see below). The low emission threshold in our BN spiky material could also be associated with the material hardness, the work function, and the ability to form sharp metallic terminations (see Figures S7 and S8).

In order to understand the unexpected and stable field emission occurring at low-turn-on voltages for the present BN nanospheres, we have investigated the electronic properties of BN ribbons exhibiting zigzag and armchair edges without hydrogen termination using the SIESTA code.[24] This code performs a fully self-consistent density functional theory (DFT) calculation by solving the standard Kohn−Sham (KS) equations. The KS orbitals are represented by a linear combination of pseudoatomic orbitals.[25] The core electrons were replaced by nonlocal norm-conserving pseudopotentials[26] in the Kleinman−Bylander factorized form.[27] A double-$\zeta$ singly polarized quality basis set[28] is employed in all calculations to represent the valence wave functions in the reciprocal space with an equivalent plane-wave mesh cutoff of 100 Ry. For the exchange and correlation potential, we use the local density approximation as proposed by Ceperley and Alder[29] in the parametrization form given by Perdrew and Zunger.[30] A set of six Monkhorst−Pack special k points[31] along the ribbon axis in the first Brillouin zone has been used for the momentum space integration. In order to prevent artificial inter-ribbon interactions, individual ribbons were separated by a sufficiently large vacuum region; both edge−edge distance and layer−layer distance were taken to be more than 10 Å. The atomic geometry was optimized using the Hellmann−Feynman forces, and the optimal lattice constant along the ribbon axis was determined by comparing the total energies. The forces acting on the individual atom were reduced to less than $10^{-3}$ eV/Å after the optimization.

First, we performed an ab initio calculation to investigate both the structural and electronic properties of an infinite BN sheet. The optimized lattice constant is 2.51 Å, and the BN sheet exhibits a direct energy gap of 4.78 eV at the K point of the two-dimensional Brillouin zone. These results are in good agreement with previous ab initio calculations[32] where the BN sheet band gap is estimated to be 4.3 eV. However, our LDA band gap is clearly underestimated when compared to the experimental band gap of bulk hexagonal BN (~5.5 eV) due to the DFT approximation, which is known to lack of accuracy in the description of the fundamental excitation gap of semiconductors or insulators.

Subsequently, we calculated the optimized atomic structures of two infinite BN ribbons whose widths were between 2.0 and 2.5 nm and exhibited zigzag and armchair edges, respectively (Figure 5). The optimized lattice constant along the ribbon axis does not change significantly from the planar BN sheet. However, some atomic reconstructions could be observed at the edges of the ribbons. For the zigzag ribbon, there is no significant structural change although the bond length between adjacent edge atoms reduces slightly to 1.4 Å. We noted that the bond length in the center of the BN ribbon is preserved (1.45 Å). However, we noted more significant structural changes for armchair edges (Figure 5) that resulted in a more pronounced decrease of the BN bond length (1.3 Å). The presence of the dangling bonds at the edges of these ribbons is responsible for inducing such a significant edge reconstruction. Although the thermal and chemical stability of these BN ribbons free from H termination has not been accurately investigated, their existence is suspected in the surface of our nanospheres during electron emission. The dehydrogenated edge is estimated to cost 3.5 eV/dangling atom in the zigzag geometry and 1.9 eV/dangling atom in the armchair one. The latter is found to be the most stable edge which could be explained by the formation of the stronger B−N bonding (1.3 Å) between dimer atoms on this specific edge.

The electronic properties of graphitic carbon ribbons without H termination,[33] as well as BN and BCN ribbons terminated by hydrogen atoms[34] have already been reported in the literature, illustrating the key role played by the edge states and the ribbon width on the energy gap of the system. However, and to the best of our knowledge, no previous theoretical study investigated the electronic properties of BN ribbons without hydrogen-termination. Consequently, the present ab initio calculations are aimed to clarify the electronic properties of these finite bare BN ribbons. The presence of free edges induces the appearance of dangling bond states (due to the hydrogen extraction). Edge states are also present, but only for the zigzag BN ribbon, similar to those observed in graphitic ribbons.[35]

In the zigzag edge case, dangling bond states appear close to the valence edge state, creating a conduction band that

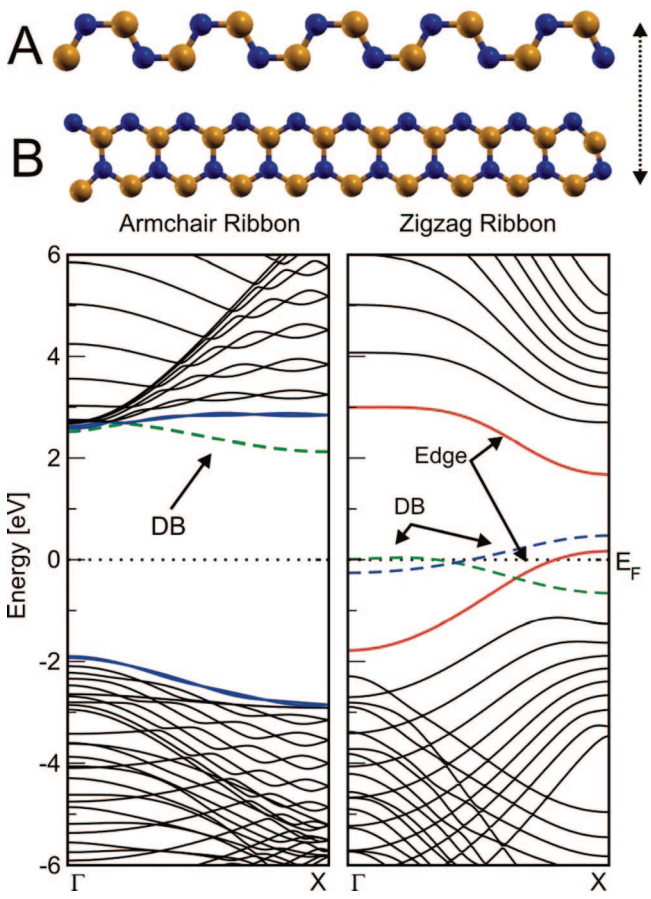


**Figure 5.** Ab initio optimized atomic configurations of two infinite BN ribbons with (A) zigzag and (B) armchair edges, respectively. Small blue and big orange circles denote N and B atoms, respectively. The unit cells of the BN ribbons with zigzag edges (A) and armchair edges (B) contain 20 and 40 atoms, respectively. The direction of the periodicity is illustrated by the dotted arrow. The corresponding band structures display a metallic behavior for zigzag and semiconducting performance for armchair ribbons. The two Fermi energies are positioned at 0 eV. Both edge and dangling bond states are indicated by arrows and denoted by "Edge" and "DB", respectively.

crosses the Fermi level, thus explaining the metallic behavior of the zigzag ribbon. In the presence of hydrogenated terminations, the same BN ribbon would have behaved like a 4 eV band gap semiconductor (close to the BN-bulk material). For the armchair ribbon, the dangling bond states appear at the bottom of the conduction band. In this case, they do not modify the semiconducting behavior of BN armchair ribbons.

The enhancement in the field emission properties can also be predicted by investigating the modification of the work function ($\varphi$) due to the presence of these dangling atoms at the ribbon edges. The work function, defined as the difference between the vacuum level and the Fermi energy, has been predicted using first-principles calculations within the macroscopic average approach.[36] In particular, the calculations were performed on: (1) a slab of six perfect BN layers (mimicking BN-bulk material), (2) a single BN sheet, (3) a H-terminated zigzag BN ribbon, and (4) a dehydrogenated zigzag BN ribbon (dangling bonds at the edges). Their corresponding work functions are $\varphi = 6.6$, 6.1, 5.6, and 5.3 eV, respectively, thus indicating that the work function of the bare zigzag BN ribbon ($\varphi = 5.3$ eV), illustrated in Figure 5, is reduced by 1.3 eV with respect to the work function of bulk BN. Consequently, such a decrease in the value of $\varphi$, induced by the presence of the edges and intensified by the dangling atoms at the ribbon's edges, explains the enhancement of the electron emission properties of the nanourchins.

The mechanism whereby electrons are emitted from these BN materials is still far from clear. However, both experimental and theoretical results suggest that active edges (BN zigzag ribbons) are needed for observing stable field emission. It is therefore possible that the metallic zigzag edges in our BN structures carry electrons and act as the emission surfaces. We believe that when the voltage is applied in the beginning of the emission, the spheres start rearranging so that electrons pass through the zigzag edges within and between the spheres (these spheres are usually coalesced and the active edges or ribbons are continuous along the surface as shown in Figure 1 and Figure S4). As the voltage increases, electrons concentrate on the metallic BN edges and emission starts and becomes stable (concentrated mainly on the sharp sites). Once the current paths are stabilized along BN edges and spikes, electrons keep emitting until the voltage is suspended.

Our calculations clearly reveal that zigzag-terminated BN ribbons exhibit an unexpected metallic behavior as illustrated in Figure 5. The position of the dangling bond states allows the presence of unoccupied states just above the Fermi energy, explaining the metallic character of these ribbons. These dangling bond states are responsible for the lower work function and are thus suspected to play a key role in the field-emission characteristics of the spiky BN structures (consisting of opened ribbons) synthesized experimentally.

We have demonstrated that it is possible to synthesize a novel type of mesoporous BN material, resembling sea urchins, using a templated method based on mesoporous carbon nanospheres. The materials were characterized using various techniques. We found that this type of material exhibits a large surface area (larger to any other BN material reported in the literature) and studied its electron emission properties. Surprisingly, we noted low-turn-on voltages, large current densities, and stable field emission in this type of nanospheres. We have attributed these results to the presence of BN ribbons protruding from the surface of the balls. With the study of the electronic properties of finite BN ribbons using sophisticated theoretical approaches, our ab initio calculations have confirmed that BN ribbons (exhibiting zigzag edges) are metallic and provided an explanation for the field emission enhancement by a reduction of the work function due to the presence of dangling bonds atoms at the ribbon edges. Further experiments using scanning tunneling microscopy and spectroscopy (STM and STS) on finite BN ribbons should now be carried out. It may also be possible to find a superconducting behavior within these ribbons. Our theoretical results clearly support our experimental observations related to the outstanding electron emission characteristics. We envisage that these novel nanomaterials may find

applications in composite fabrication, gas adsorption devices, catalysts, and field-emission systems.

**Acknowledgment.** This work was sponsored by CONACYT-México Grants 56787 (Laboratory for Nanoscience and Nanotechnology Research-LINAN), 45762 (H.T.), 45772 (M.T.), 41464-Inter American Collaboration (M.T.), 42428-Inter American Collaboration (H.T.), 2004-01-013/SALUD-CONACYT (M.T.), Fondo Mixto de San Luis Potosí 63001 S-3908 (M.T.). The authors are also grateful to D. Ramírez González, Lisette Noyola, and Grisel Ramírez-Manzanares for technical assistance. J.C.C. is indebted to FNRS of Belgium for financial support. Parts of this work are also directly connected to the Belgian Program on Interuniversity Attraction Poles (PAI), to the ARC sponsored by the Communauté Française de Belgique, and to the NANOQUANTA and FAME European Networks of Excellence.

**Supporting Information Available:** TEM and HAADF images of BN nanospheres and a pore diameter distribution plot of BN nanospheres. This material is available free of charge via the Internet at http://pubs.acs.org.

## References

(1) Terrones, M.; Grobert, N.; Terrones, H. *Carbon* **2002**, *40*, 1665–1684.
(2) Ma, R. Z.; Golberg, D.; Bando, Y.; Sasaki, T. *Philos. Trans. R. Soc. London, Ser. A* **2004**, *362*, 2161–2187.
(3) Terrones, M.; Romo-Herrera, J. M.; Cruz-Silva, E.; López-Urías, F.; Muñoz-Sandoval, E.; Velázquez-Salazar, J. J.; Terrones, H.; Bando, Y.; Golberg, D. *Mater. Today* **2007**, *10*, 30–38.
(4) Chopra, N. G.; Luyken, R. J.; Cherrey, K.; Crespi, V. H.; Cohen, M. L.; Louie, S. G.; Zettl, A. *Science* **1995**, *269*, 966–967.
(5) Loiseau, A. N.; Hug, G.; Pascard, H. *Phys. Rev. Lett.* **1996**, *76*, 4737–4740.
(6) Terrones, M.; Hsu, W. K.; Terrones, H.; Zhang, J. P.; Ramos, S.; Hare, J. P.; Castillo, R.; Prassides, K.; Cheetham, A. K.; Kroto, H. W.; Walton, D. R. M. *Chem. Phys. Lett.* **1996**, *259*, 568–573.
(7) Han, W. Q.; Bando, Y.; Kurashima, K.; Sato, T. *Appl. Phys. Lett.* **1998**, *73*, 3085–3087.
(8) Chen, Y.; Chadderton, L. T.; Gerald, J. F.; Williams, J. S. *Appl. Phys. Lett.* **1999**, *74*, 2960–2962.
(9) Velázquez-Salazar, J. J.; Muñoz-Sandoval, E.; Romo-Herrera, J. M.; Lupo, F.; Rühle, M.; Terrones, H.; Terrones, M. *Chem. Phys. Lett.* **2005**, *416*, 342–348.
(10) Golberg, D.; Bando, Y.; Eremets, M.; Takemura, K.; Kurashima, K.; Tamiya, H.; Yusa, H. *Chem. Phys. Lett.* **1997**, *279*, 191–196.
(11) Cumings, J.; Zettl, A. *Sol. St. Commun.* **2004**, *129*, 661–664.
(12) Domínguez, J. M.; Terrés, E.; Vázquez, A. *Microporous Mesoporous Mater.* **2003**, *66*, 341–348.
(13) Golberg, D.; Bando, Y.; Kurashima, K.; Sato, T. *Chem. Phys. Lett.* **2000**, *323*, 185–191.
(14) Golberg, D.; Bando, Y.; Kurashima, K.; Sato, T. *Sol. St. Commun.* **2000**, *116*, 1–6.
(15) Han, W. Q.; Brutchey, R.; Tilley, T. D.; Zettl, A. *Nano Lett.* **2004**, *4*, 173–176.
(16) Terrés, E.; Panella, B.; Hayashi, T.; Kim, Y. A.; Endo, M.; Dominguez, J. M.; Hirscher, M.; Terrones, H.; Terrones, M. *Chem. Phys. Lett.* **2005**, *403*, 363–366.
(17) Hu, S.; Kan, E. J.; Yang, J. *J. Chem. Phys.* **2007**, *127*, 164718.
(18) Cheng, J.; Ding, R.; Liu, Y.; Ding, Z.; Zhang, L. *Comput. Mater. Sci.* **2007**, *40*, 341–344.
(19) Ma, R. Z.; Bando, Y.; Sato, T.; Golberg, D.; Zhu, H.; Xu, C.; Wu, D. *Appl. Phys. Lett.* **2002**, *81*, 5225–5227.
(20) Lim, S. H.; Luo, J.; Ji, W.; Lin, J. *Catal. Today* **2007**, *120*, 346–350.
(21) Sugino, T.; Kimura, C.; Yamamoto, T. *Appl. Phys. Lett.* **2002**, *80*, 3602–3604.
(22) Rinzler, A. G.; Hafner, J. H.; Nikolaev, P.; Lou, L.; Kim, S. G.; Tomanek, D.; Nordlander, P.; Colbert, D. T.; Smalley, R. E. *Science* **1995**, *269*, 1550–1553.
(23) Bonard, J.-M.; Kind, H.; Stockli, T.; Nilsson, L.-O. *Solid-State Electron.* **2001**, *45*, 893–914.
(24) Soler, J. M.; Artacho, E.; Gale, J. D.; García, A.; Junquera, J.; Ordejón, P.; Sánchez-Portal, D. *J. Phys.: Condens. Matter* **2002**, *14*, 2745–2780.
(25) Sankey, O. F.; Niklewski, D. J. *Phys. Rev. B* **1989**, *40*, 3979–3995.
(26) Troullier, N.; Martins, J. L. *Phys. Rev. B* **1991**, *43*, 1993–2006.
(27) Kleinman, L.; Bylander, D. M. *Phys. Rev. Lett.* **1982**, *48*, 1425–1428.
(28) Junquera, J.; Paz, O.; Sánchez-Portal, D.; Artacho, E. *Phys. Rev. B* **2001**, *64*, 235111.
(29) Ceperley, D. M.; Alder, B. J. *Phys. Rev. Lett.* **1980**, *45*, 566–569.
(30) Perdew, J.; Zunger, A. *Phys. Rev. B* **1981**, *23*, 5048–5079.
(31) Monkhorst, H. J.; Pack, J. D. *Phys. Rev. B* **1976**, *13*, 5188–5192.
(32) Blase, X.; Rubio, A.; Louie, S. G.; Cohen, M. L. *Phys. Rev. B* **1995**, *51*, 6868–6875.
(33) Kawai, T.; Miyamoto, Y.; Sugino, O.; Koga, Y. *Phys. Rev. B* **2000**, *62*, R16349–16352.
(34) Nakamura, J.; Nitta, T.; Natori, A. *Phys. Rev. B* **2005**, *72*, 205429.
(35) Nakada, K.; Fujita, M.; Dresselhaus, G.; Dresselhaus, M. S. *Phys. Rev. B* **1996**, *54*, 17954–1796.
(36) Baldereschi, A.; Baroni, S.; Resta, R. *Phys. Rev. Lett.* **1998**, *61*, 734–737.

NL072713M